

## Article

# Succinyl and Adipoyl Dihydrazones: A Solid-State, Solution and Antibacterial Study

Edi Topić <sup>1</sup> , Vladimir Damjanović <sup>2</sup>, Katarina Pičuljan <sup>1</sup>, Višnja Vrdoljak <sup>1</sup>  and Mirta Rubčić <sup>1,\*</sup><sup>1</sup> Department of Chemistry, Faculty of Science, University of Zagreb, Horvatovac 102a, 10000 Zagreb, Croatia<sup>2</sup> Department of Chemistry and Biochemistry, School of Medicine, University of Zagreb, Šalata 3, 10000 Zagreb, Croatia

\* Correspondence: mirta@chem.pmf.hr; Tel.: +385-1-4606-374

**Abstract:** A series of aryl-functionalized alkyl dihydrazones was prepared by condensation of succinyl or adipoyl dihydrazide and selected *ortho*-hydroxybenzaldehydes (2-hydroxybenzaldehyde, 2-hydroxy-1-naphthaldehyde, 2,3-dihydroxybenzaldehyde, and 2,4-dihydroxybenzaldehyde) in solution. The obtained products were structurally characterized in the solid state by single-crystal X-ray diffraction (SC-XRD), thermal analysis (TGA-DSC), and Fourier transform infrared (FTIR) spectroscopy and in DMSO-*d*<sub>6</sub> solution by nuclear magnetic resonance (NMR) techniques. Combined FTIR and crystal structure data point to a N–NH–C=O tautomeric form of the hydrazone parts as well as the enol-imino tautomeric form of the aldehyde residues and a robust *trans-syn* conformation for the structurally investigated ones. While the molecules retain the same tautomeric form in the DMSO-*d*<sub>6</sub> solution, they adopt several conformations, due to rotations around C<sub>ar</sub>–C, C–N, and N–N bonds. The compounds show exceptional thermal stability, with a complex degradation pattern. Slight differences in thermal behavior correlate to alkyl chain length and aryl substituents. The *in vitro* cytotoxic activity of prepared dihydrazones was evaluated on THP-1 and HepG2 cell lines, while their antibacterial activity was tested against *Staphylococcus aureus*, *Enterococcus faecalis*, *Escherichia coli*, and *Moraxella catarrhalis* bacteria. All compounds proved to be non-cytotoxic, and some exhibited moderate antibacterial activity.

**Keywords:** hydrazones; tautomerism; structural analysis; NMR spectroscopy; antibacterial activity



**Citation:** Topić, E.; Damjanović, V.; Pičuljan, K.; Vrdoljak, V.; Rubčić, M. Succinyl and Adipoyl Dihydrazones: A Solid-State, Solution and Antibacterial Study. *Crystals* **2022**, *12*, 1175. <https://doi.org/10.3390/cryst12081175>

Academic Editor: Raghvendra Singh Yadav

Received: 31 July 2022

Accepted: 18 August 2022

Published: 21 August 2022

**Publisher's Note:** MDPI stays neutral with regard to jurisdictional claims in published maps and institutional affiliations.



**Copyright:** © 2022 by the authors. Licensee MDPI, Basel, Switzerland. This article is an open access article distributed under the terms and conditions of the Creative Commons Attribution (CC BY) license (<https://creativecommons.org/licenses/by/4.0/>).

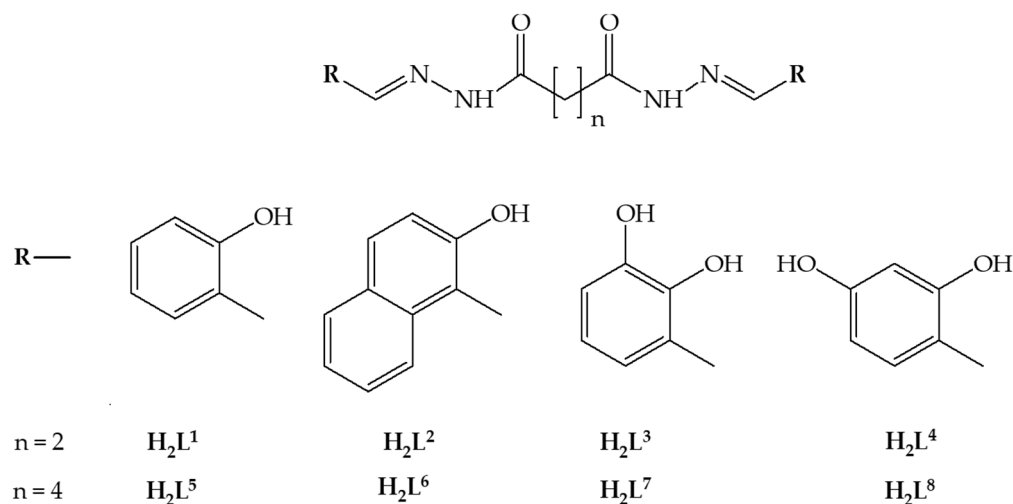
## 1. Introduction

In the last few decades, hydrazones have emerged as a class of compounds associated with a multitude of specific functions [1–3]. Owing to the stability, modularity, and acid-base properties of the hydrazone R<sub>1</sub>R<sub>2</sub>C=N–NHR<sub>3</sub> linkage, such systems have been well acclaimed as anion receptors [4], sensors [5], and molecular switches [6]. On the other hand, compounds of this kind have shown biological activities relevant to the treatment of different conditions, such as inflammation, cancer, or Alzheimer's disease [7–13]. Moreover, their propensity to isomerization makes them appropriate for the construction of metal-organic assemblies, which have been extensively investigated for their biological and catalytic potential [14–16].

The introduction of more than one hydrazone subunit within the same molecule can give superior functions, e.g., sensor action, bioactivity, or binding capacity, in comparison with the monohydrazone compounds [17,18]. This is intrinsically related to greater isomeric and tautomeric prosperity as well as redox activity of the systems [19–21]. Such behavior can be even more pronounced if the molecular fragments connecting hydrazone subunits are flexible (e.g., alkyl joints), as they allow spatially separated hydrazone parts to approach closely [18,22,23].

Development of novel antibacterial agents or modification of existing ones is nowadays one of the vital directions in medicinal chemistry, where hydrazone scaffolds are

considered as promising candidates [10,24,25]. While most such studies have been devoted to monohydrazone compounds (Supplementary Materials, Scheme S1), those evaluating derivatives with two or more hydrazone subunits are less numerous and mostly targeted at their metal complexes [26–29]. Against this background, we chose to explore succinyl- and adipoyl-based dihydrazones, enumerated in Scheme 1, in the solid state and in solution, while complementing their behavior with cytotoxic and antibacterial activity assays.



**Scheme 1.** The succinyl- and adipoyl-based dihydrazones.

In the present study, we unveil efficient synthetic protocols towards the title compounds, accompanied by a thorough solid-state analysis of the resulting compounds via Fourier transform infrared (FTIR) spectroscopy, simultaneous thermogravimetric analysis and differential scanning calorimetry (TGA-DSC), and X-ray diffraction (XRD). A detailed nuclear magnetic resonance (NMR) study revealed that, in DMSO-*d*<sub>6</sub> solution, all compounds offered several isomers, while their hydrazone subunits assumed the same tautomeric form as established in the solid state. Finally, the examined dihydrazones proved to be non-cytotoxic, while some of the derivatives showed moderate antibacterial activity against the selected bacterial strains.

## 2. Materials and Methods

### 2.1. Synthesis

Succinic dihydrazide, adipic dihydrazide, salicylaldehyde, 2,3-dihydroxybenzaldehyde, 2,4-dihydroxybenzaldehyde, and 2-hydroxy-1-naphthaldehyde were purchased from TCI and used as received. Ethanol, used in syntheses, was purchased from Kemika (Zagreb, Croatia).

Dihydrazones were prepared by condensation of two equivalents of aldehyde with one equivalent of alkyl dihydrazide in boiling ethanol by the following general procedure: 2.0 mmol of aldehyde was dissolved in 20 mL of hot ethanol. Then, 1.0 mmol of appropriate alkyl dihydrazide was added as a solid to the solution. The resulting suspension was refluxed for two hours with vigorous stirring. After cooling, the solids were filtered and dried on air.

#### 2.1.1. Synthesis of H<sub>4</sub>L<sup>1</sup>

Obtained by the reaction of salicylaldehyde and succinic dihydrazide. Yield: 0.29 g (82%). White powder. Anal. Calcd. for C<sub>18</sub>H<sub>18</sub>N<sub>4</sub>O<sub>4</sub> (354.39): C, 61.00%, H, 5.12%, N, 15.81%. Found: C, 61.19%, H, 4.87%, N, 15.40%. IR spectroscopy: 1670, 1651  $\nu$ (C=O); 1621, 1608  $\nu$ (C=N); 1573  $\nu$ (C=C); 1486  $\delta$ (N–H); 1268  $\nu$ (C(O)–N); 1203  $\nu$ (C–O). <sup>1</sup>H NMR:  $\delta$  8.29, 8.35, 10.13, 10.14, 11.17, 11.21, 11.28, 11.29, 11.7, 11.72. <sup>13</sup>C NMR:  $\delta$  141.4, 141.5, 146.7, 146.9, 156.7, 157.7, 168.1, 168.4, 173.4, 173.5. <sup>15</sup>N NMR:  $\delta$  174, 179.2, 302.5, 312. Detailed assignment in the Supplementary Material.

### 2.1.2. Synthesis of H<sub>4</sub>L<sup>2</sup>

Obtained by the reaction of 2-hydroxy-1-naphthaldehyde and succinic dihydrazide. Yellow powder. Yield: 0.28 g (62%). Anal. Calcd. for C<sub>26</sub>H<sub>22</sub>N<sub>4</sub>O<sub>4</sub> (454.51): C, 68.70%, H, 4.88%, N, 12.33%. Found: C, 68.41%, H, 4.59%, N, 11.88%. IR (ATR, cm<sup>-1</sup>): 1660 ν(C=O); 1623 ν(C=N); 1595 ν(C=C); 1467 δ(N-H); 1279 ν(C(O)-N); 1204 ν(C-O). <sup>1</sup>H NMR: δ 8.93, 8.96, 9.16, 9.18, 11.14, 11.18, 11.3, 11.38, 11.76, 11.83, 11.85, 12.59, 12.61, 12.63. <sup>13</sup>C NMR: δ 142.7, 142.8, 145.1, 145.2, 145.3, 158.2, 167.9. <sup>15</sup>N NMR: δ 173.4, 179.6, 296.3, 307.7. Detailed assignment in the Supplementary Material.

### 2.1.3. Synthesis of H<sub>4</sub>L<sup>3</sup>

Obtained by the reaction of 2,3-dihydroxybenzaldehyde and succinic dihydrazide. Yield: 0.24 g (62%). Off-white powder. Anal. Calcd. for C<sub>18</sub>H<sub>18</sub>N<sub>4</sub>O<sub>6</sub> (386.39): C, 55.95%, H, 4.70%, N, 14.50%. Found: C, 55.72%, H, 4.96%, N, 14.19%. IR (ATR, cm<sup>-1</sup>): 1669, 1642 ν(C=O); 1623, 1612 ν(C=N); 1587 ν(C=C); 1471 δ(N-H); 1268 ν(C(O)-N); 1205 ν(C-O). <sup>1</sup>H NMR: δ 8.26, 8.27, 8.31, 9.16, 9.17, 9.43, 9.45, 9.48, 9.53, 11.01, 11.06, 11.3, 11.31, 11.7, 11.72. <sup>13</sup>C NMR: δ 142.4, 142.5, 145.6, 146.4, 147.6, 168, 168.3, 173.2, 173.4. <sup>15</sup>N NMR: δ 172.4, 179, 301, 310. Detailed assignment in the Supplementary Material.

### 2.1.4. Synthesis of H<sub>4</sub>L<sup>4</sup>

Obtained by the reaction of 2,4-dihydroxybenzaldehyde and succinic dihydrazide. Yield: 0.27 g (70%). Off-white powder. The sample was dried before elemental analysis. Anal. Calcd. for C<sub>18</sub>H<sub>18</sub>N<sub>4</sub>O<sub>6</sub> (386.39): C, 55.95%, H, 4.70%, N, 14.5%. Found: C, 56.01%, H, 4.70%, N, 14.14%. IR (ATR, cm<sup>-1</sup>): 1651 ν(C=O); 1628, 1613 ν(C=N); 1590 ν(C=C), 1472 δ(N-H); 1270 ν(C(O)-N); 1221 ν(C-O). <sup>1</sup>H NMR: δ 8.13, 8.14, 8.21, 9.89, 10.15, 11.09, 11.1, 11.35, 11.48, 11.51. <sup>13</sup>C NMR: δ 142.8, 147.7, 147.8, 158.6, 159.8, 160.7, 161, 167.7, 167.9, 172.8, 173. <sup>15</sup>N NMR: δ 172, 177.8, 291, 300. Detailed assignment in the Supplementary Material.

### 2.1.5. Synthesis of H<sub>4</sub>L<sup>5</sup>

Obtained by the reaction of salicylaldehyde and adipic dihydrazide. White powder. Yield: 0.28 g (73%). Anal. Calcd. for C<sub>20</sub>H<sub>22</sub>N<sub>4</sub>O<sub>4</sub> (382.44): C, 62.81%, H, 5.80%, N, 14.65%. Found: C, 62.84%, H, 5.61%, N, 14.83%. IR (ATR, cm<sup>-1</sup>): 1664 ν(C=O); 1610 ν(C=N); 1556 ν(C=C); 1489 δ(N-H); 1273 ν(C(O)-N); 1219 ν(C-O). <sup>1</sup>H NMR: δ 8.27, 8.35, 10.13, 11.2, 11.22, 11.58, 11.6. <sup>13</sup>C NMR: δ 141.2, 147, 156.8, 157.8, 168.7, 174.1, 174.2. <sup>15</sup>N NMR: δ 174.4, 180.6, 303, 312.7. Detailed assignment in the Supplementary Material.

### 2.1.6. Synthesis of H<sub>4</sub>L<sup>6</sup>

Obtained by the reaction of 2-hydroxy-1-naphthaldehyde and adipic dihydrazide. Yellow powder. Yield: 0.29 g (60%). Anal. Calcd. for C<sub>28</sub>H<sub>26</sub>N<sub>4</sub>O<sub>4</sub> (482.56): C, 69.69%, H, 5.43%, N, 11.61%. Found: C, 69.92%, H, 5.72%, N, 11.42%. IR (ATR, cm<sup>-1</sup>): 1654 ν(C=O); 1621 ν(C=N); 1570, 1551 ν(C=C); 1466 δ(N-H); 1282 ν(C(O)-N); 1240 ν(C-O). <sup>1</sup>H NMR: δ 8.93, 8.94, 9.12, 9.17, 11.3, 11.7, 12.6. <sup>13</sup>C NMR: δ 142.7, 145.4, 157.3, 158.6, 168.6, 173.7. <sup>15</sup>N NMR: δ 174.3, 180.6, 296.1, 308.1. Detailed assignment in the Supplementary Material.

### 2.1.7. Synthesis of H<sub>4</sub>L<sup>7</sup>

Obtained by the reaction of 2,3-dihydroxybenzaldehyde and adipic dihydrazide. Off-white powder. Yield: 0.18 g (43%). Anal. Calcd. for C<sub>20</sub>H<sub>22</sub>N<sub>4</sub>O<sub>6</sub> (414.44): C, 57.96%, H, 5.35%, N, 13.52%. Found: C, 57.67%, H, 5.60%, N, 13.37%. IR (ATR, cm<sup>-1</sup>): 1652 ν(C=O); 1612 ν(C=N); 1564 ν(C=C); 1488 δ(N-H); 1258 ν(C(O)-N); 1220 ν(C-O). <sup>1</sup>H NMR: δ 8.25, 8.3, 9.43, 9.44, 9.46, 11.07, 11.08, 11.22, 11.23, 11.61. <sup>13</sup>C NMR: δ 142.2, 145.6, 145.9, 146.4, 147.8, 168.7, 174.1, 177. <sup>15</sup>N NMR: δ 174.5, 179.9, 300.9, 311.3. Detailed assignment in the Supplementary Material.

### 2.1.8. Synthesis of H<sub>4</sub>L<sup>8</sup>

Obtained by the reaction of 2,4-dihydroxybenzaldehyde and adipic dihydrazide. Off-white powder. Yield: 0.16 g (39%). Anal. Calcd. for C<sub>20</sub>H<sub>22</sub>N<sub>4</sub>O<sub>6</sub> (414.44): C, 57.96%, H, 5.35%, N, 13.52%. Found: C, 58.42%, H, 5.40%, N, 13.53%. IR (ATR, cm<sup>-1</sup>): 1673  $\nu$ (C=O); 1629, 1606  $\nu$ (C=N); 1561  $\nu$ (C=C); 1447  $\delta$ (N–H); 1268  $\nu$ (C(O)–N); 1216  $\nu$ (C–O). <sup>1</sup>H NMR:  $\delta$  8.13, 8.22, 10, 11, 11.03, 11.4, 11.43. <sup>13</sup>C NMR:  $\delta$  142.6, 147.9, 158.5, 159.8, 160.7, 161, 168.4, 173.7. <sup>15</sup>N NMR:  $\delta$  173.4, 178.4, 291.5, 300.8. Detailed assignment in the Supplementary Material.

### 2.2. Methods

Elemental analyses (C, H, N) were provided by the Analytical Services Laboratory of the Ruđer Bošković Institute, Zagreb, Croatia. Powder patterns of the samples were collected on a Panalytical Empyrean diffractometer (Panalytical, Almelo, The Netherlands) using Cu K $\alpha$  radiation, PIXcel3D detector, and automatic divergent optics on zero-background sample holders in Bragg–Brentano geometry. The patterns were collected in the  $2\theta$  range between 4° and 40°, with a step size of 0.0066° and counting time of 32.7 s/px. Data were evaluated using X'Pert Highscore v4.9 software (Panalytical, Almelo, The Netherlands). FTIR ATR attenuated total reflectance spectra were recorded on a Nicolet iS50 spectrometer (Thermo Scientific, Waltham, MA, USA) equipped with diamond ATR stage in the spectral range of 4000 to 400 cm<sup>-1</sup>. A total of 16 scans were co-added for each spectrum at 1 cm<sup>-1</sup> resolution, with a total acquisition time of ~30 s. Data were evaluated using OMNIC software (version 8, Thermo Scientific, Waltham, MA, USA). Combined thermogravimetric analyses/differential scanning calorimetry (TGA/DSC) was conducted on a Mettler-Toledo TGA/DSC 3+ thermobalance (Mettler-Toledo, Columbus, SAD) with aluminium crucibles under dynamic nitrogen stream of 50 mL min<sup>-1</sup> in a temperature range between 25 °C and 300 °C, while the heating rate was set to 10 °C·min<sup>-1</sup>. The results of experiments were processed with Mettler Toledo STARe Evaluation Software (version 16.10, Mettler-Toledo, Columbus, SAD).

High-quality single crystals of H<sub>4</sub>L<sup>4</sup>·2H<sub>2</sub>O, H<sub>4</sub>L<sup>6</sup> and H<sub>4</sub>L<sup>7</sup> were grown from the DMSO solutions. Diffracted intensities were collected on a Rigaku XtaLAB Synergy diffractometer (Rigaku Oxford Diffraction: Oxford, UK) equipped with Dualflex source (Cu K $\alpha$  radiation,  $\lambda$  = 1.54184 Å) and a HyPix detector using  $\omega$ -scans. The crystal was kept at 170 K during data collection. Data were prepared using the CrysAlis program package (1.171.41.92a; Rigaku Oxford Diffraction: Oxford, UK) [30]. A summary of general and crystal data, intensity data collection, and final refinement parameters is presented in Table S1 (Supplementary Material). The structures were solved with dual space methods using SHELXT [31]. The refinement procedure by full-matrix least-squares methods based on  $F^2$  values against all reflections included anisotropic displacement parameters for all non-H atoms. Hydrogen atoms bound to carbon atoms were placed in geometrically idealized positions and refined by the use of the riding model with  $U_{\text{iso}} = 1.2U_{\text{eq}}$  of the connected carbon atom or as ideal CH<sub>3</sub> groups with  $U_{\text{iso}} = 1.5U_{\text{eq}}$ . Hydrogen atoms attached to heteroatoms were located in the difference Fourier maps at the final stages of the refinement procedure. Their coordinates were refined freely but with restrained N–H distances of 0.86(2) and O–H distances of 0.82(2) Å. All refinements were performed using SHELXL [32]. The SHELX programs operated within the Olex2 suite [33]. Geometrical calculations and molecular graphics were performed with Mercury [34]. Crystals of other compounds/solid phases were found unsuitable for single-crystal diffraction analysis due to small size and/or low crystal quality.

**NMR spectroscopy.** 1D (<sup>1</sup>H, <sup>13</sup>C-DEPTq) and 2D (COSY, <sup>1</sup>H-<sup>13</sup>C HSQC, <sup>1</sup>H-<sup>13</sup>C HMBC, <sup>1</sup>H-<sup>15</sup>N HSQC, <sup>1</sup>H-<sup>15</sup>N HMBC) solution-state NMR spectra were recorded on a Bruker Avance III HD 400 MHz/54 mm Ascend spectrometer (Bruker, Billerica, USA) equipped with a 5 mm PA BBI 1H/D BB Z-GRAD probehead using standard Bruker pulse programs in the range of 25 °C to 75 °C. DMSO-*d*<sub>6</sub> was used as solvent and TMS as an

internal standard for proton and carbon chemical shifts. Nitrogen chemical shifts were extracted from 2D  $^1\text{H}$ - $^{15}\text{N}$  HSQC/HMBC spectra and reported relative to liquid ammonia.

**In vitro biological studies.** The cytotoxic properties of examined dihydrazones were tested against acute monocytic leukemia (THP-1, ATCC TIB-202) and hepatocellular carcinoma (HepG2, ATCC HB-8065) human cell lines using the MTS assay [35] according to the protocol that was provided in a previous study [36]. Their antibacterial activity was tested as described previously [36] against two Gram-positive, i.e., *Staphylococcus aureus* (ATCC 29213) and *Enterococcus faecalis* (ATCC 29212), and two Gram-negative, i.e., *Escherichia coli* (ECM 1556) and *Moraxella catarrhalis* (ATCC 23246), bacterial strains by the broth microdilution method and according to CLSI guidelines [37].

### 3. Results and Discussion

#### 3.1. Synthesis and Solid-State Characterization

Synthesis of the title compounds was achieved by condensation of alkyl dihydrazide and the appropriate aldehyde in a 1:2 molar ratio and proceeded straightforwardly. Ethanol was chosen as the ecologically most benign solvent, although syntheses can be performed in, e.g., methanol with comparable outcomes. Since the starting alkyl dihydrazides and resulting dihydrazones are poorly soluble in any solvent other than DMSO, to assure reaction completion, mixtures were vigorously stirred and heated for two hours.

Except for  $\text{H}_4\text{L}^4$ , which crystallizes as the dihydrate, i.e.,  $\text{H}_4\text{L}^4 \cdot 2\text{H}_2\text{O}$ , as determined by X-ray diffraction (vide infra), analysis of the remaining members of this series gave no concrete evidence for the presence of crystal solvents and were treated as essentially non-solvated.  $\text{H}_4\text{L}^4 \cdot 2\text{H}_2\text{O}$  is not stable at ambient conditions and starts to lose crystal water after exposure to such conditions (Supplementary Material, Figure S4), while the other compounds show a mostly featureless and flat  $m(T)$  curve up to 170 °C (Figure 1, Supplementary Material, Figures S1–S9). Nevertheless, prepared dihydrazones show an interesting contrast in thermal behavior above 170 °C. Even though all of the investigated compounds show relatively high thermal stability, those derived from succinic dihydrazide start decomposing at around 200 °C, while the ones derived from adipic dihydrazide exhibit much higher decomposition onset points at around 270 °C. It must be pointed out that TG and DSC curves reveal that these compounds do not simply melt but experience complex phase transitions and degradation processes upon heating (Supplementary Material, Figures S1–S8), in some cases coupled with several endo- and exothermic events, as seen for  $\text{H}_4\text{L}^4$  (Supplementary Material, Figure S4, Note S1). It should be noted that the observed patterns seen on the DSC curves do not seem to reflect straightforwardly the nature of the aldehydic or hydrazonic residues of the investigated compounds. Indeed, in-depth insight into the pathways and mechanisms of thermal degradation for the investigated compounds will require a significant experimental and theoretical effort. Similar complexity in thermal behavior was previously established for a series of carbohydrazides, close relatives of compounds investigated here [36,38]. Finally, it is interesting to note that compounds derived from dihydroxybenzaldehydes are not so resilient to heating as their salicylaldehyde or naphthaldehyde counterparts.

**FTIR spectroscopy.** All FTIR-ATR spectra (Supplementary Material, Figures S10–S17) of the investigated compounds are fairly similar and strongly suggest that all isolated compounds exist in the solid state in the same tautomeric form, the enol-imino one, when considering aldehyde residues, and have their hydrazone linkages in the N–NH–C=O form. In all cases, the spectra are characterized by a set of superimposed bands in the region between  $\approx 2800\text{ cm}^{-1}$  and  $\approx 3500\text{ cm}^{-1}$ , which are assigned to stretching of N–H, O–H, and C–H functionalities. Stretching vibrations of the amide C=O group (amide I band) are observed around  $1660\text{ cm}^{-1}$ , while the stretching vibrations of the imine C=N and the C=C<sub>ar</sub> moieties of the aldehyde residues appear at  $\approx 1620\text{ cm}^{-1}$  and  $\approx 1550\text{ cm}^{-1}$ , respectively. Comparing the position of the amide I band in the spectra of  $\text{H}_4\text{L}^1$ – $\text{H}_4\text{L}^8$  with those observed for similar compounds suggests the involvement of the C=O moiety in extensive hydrogen bonding [36,38,39]. For  $\text{H}_4\text{L}^2$ ,<sup>39</sup>  $\text{H}_4\text{L}^4$ ,  $\text{H}_4\text{L}^6$ , and  $\text{H}_4\text{L}^7$ , this is

unambiguously confirmed by structural studies via X-ray diffraction (*vide infra*). Finally, the bands arising from the N–H deformations appear at ca.  $1470\text{ cm}^{-1}$ , whereas the stretching vibrations of the C(O)–N and C–O functionalities are found at  $\approx 1260\text{ cm}^{-1}$  and  $\approx 1210\text{ cm}^{-1}$ , respectively.

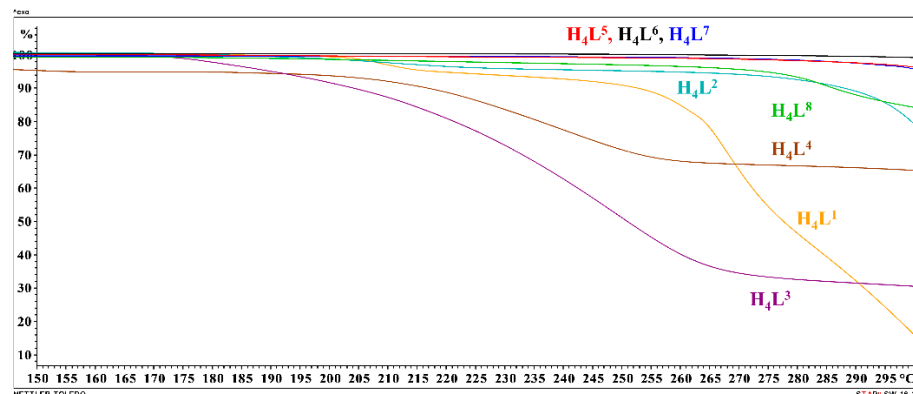


**Figure 1.** Comparison of TG curves for dihydrazones on the common scale. Dihydrazones derived from succinic dihydrazide show significantly lower thermal stability.

**Single-crystal X-ray diffraction.** During this study,  $\text{H}_4\text{L}^2\cdot\text{DMSO}$ ,  $\text{H}_4\text{L}^4\cdot 2\text{H}_2\text{O}$ ,  $\text{H}_4\text{L}^6$ , and  $\text{H}_4\text{L}^7$  were obtained in the form of crystals of suitable size and quality for single-crystal X-ray diffraction experiments (Supplementary Materials, Figures S18–S21). The measured crystal structure of  $\text{H}_4\text{L}^2\cdot\text{DMSO}$  is essentially identical to the one reported in the literature (Supplementary Materials, Note S2) [39]. Careful analysis of relevant bond lengths and angles (Supplementary Materials, Tables S2 and S3) reveals that the investigated compounds assume a N–NH–C=O form, considering their hydrazone parts, while the aldehyde parts exist in the enol-imino form (Figure 2). As expected for arylhydrazones derived from *ortho*-hydroxybenzaldehydes, an intramolecular hydrogen bond O1–H1...N1 stabilizing the molecular structures is established in all cases, while the molecules adopt *trans-syn* conformation (Supplementary Material, Table S4, Figures S22–S31). Nevertheless, there are subtle conformational differences in the molecular structures of the investigated compounds, with  $\text{H}_4\text{L}^7$  showing centrosymmetric geometry,  $\text{H}_4\text{L}^6$  revealing two symmetrically independent but still centrosymmetric molecules (one being planar and the other skewed), and  $\text{H}_4\text{L}^4$  failing to achieve inversion symmetry due to slight canting of the aryl rings. In the case of  $\text{H}_4\text{L}^6$  and  $\text{H}_4\text{L}^7$ , which contain planar molecules, the distance between the two coplanar subunits of dihydrazone ligands is  $\approx 0.77\text{ \AA}$  for  $\text{H}_4\text{L}^7$  and  $\approx 0.68\text{ \AA}$  for the planar molecule of  $\text{H}_4\text{L}^6$ . The skewed molecule of  $\text{H}_4\text{L}^6$  has an interplanar angle of the phenyl rings only ca.  $2^\circ$ , but its interring distance is considerably shorter than in the planar molecule:  $16.8\text{ \AA}$  vs.  $19.4\text{ \AA}$ , respectively. It seems reasonable that a combination of planar and skewed molecules in the crystal structure facilitates the packing of bulky naphthyl substituents. Similarly, aryl subunits in  $\text{H}_4\text{L}^4$  are not coplanar, forming an angle of ca.  $6^\circ$ , with a shorter intercentroid distance of  $15.8\text{ \AA}$  due to a shorter alkyl linker.

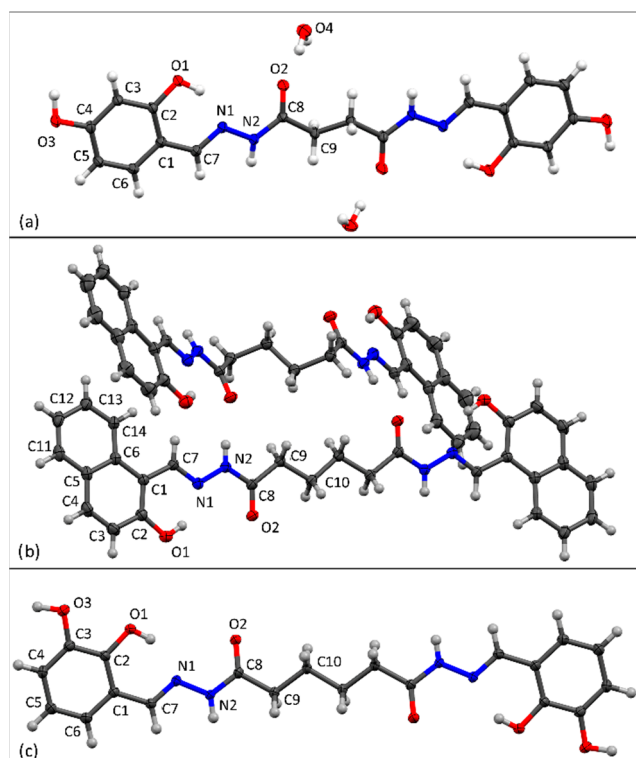


**Figure 2.** Molecular structures of: (a)  $\text{H}_4\text{L}^4 \cdot 2\text{H}_2\text{O}$ , (b)  $\text{H}_4\text{L}^6$ , and (c)  $\text{H}_4\text{L}^7$  with the atom numbering schemes. Displacement ellipsoids are drawn at the 50% probability level. Hydrogen atoms are presented as spheres of arbitrarily small radii.

Crystal packing in  $\text{H}_4\text{L}^4 \cdot 2\text{H}_2\text{O}$ ,  $\text{H}_4\text{L}^6$ , and  $\text{H}_4\text{L}^7$  are dominated by hydrogen bonds established between the amide functionalities ( $-\text{NH}-\text{C}=\text{O}$ ) of the molecules and remaining available hydrogen donors and acceptors (Figure 3; Supplementary Material, Table S4, Figures S32–S36). In  $\text{H}_4\text{L}^7$ , only two hydrogen bond motifs are achieved, one being a  $C_1^1(10)$  chain formed between a  $\text{C}=\text{O}$  amide fragment and the 3-hydroxy group of an aryl fragment and the other being a  $C_1^1(7)$  chain between an amide N-H moiety and the 2-hydroxy group of an aryl fragment [40]. However, these two simple interactions combine, affording complex hydrogen-bonded networks, such as a supramolecular  $R_8^8(60)$  ring consisting of only the  $C_1^1(10)$  chain motif, a  $R_6^6(70)$  supramolecular ring comprising the  $C_1^1(7)$  chain motif only, and various supramolecular rings when the two motifs are considered in combination. In  $\text{H}_4\text{L}^6$ , hydrogen bonding scenarios are a bit simpler, as only the amide fragments can interact. Here, the main supramolecular motif is a  $C_4^4(26)$  chain consisting of two pairs of symmetrically independent molecules interacting through amide subunits. Finally, the crystal structure of  $\text{H}_4\text{L}^4 \cdot 2\text{H}_2\text{O}$  shows quite a rich variety of hydrogen bond motifs due to the presence of water molecules. The supramolecular structure can be satisfactorily described as a layered one, relying on hydroxy functional groups and water molecules as hydrogen bond donors and the amide  $\text{C}=\text{O}$  groups and, again, water molecules as hydrogen bond acceptors. The *para*-hydroxy group is responsible for building the layer, forming, among others, a  $R_6^6(78)$  supramolecular ring motif, while the interaction of an *ortho*-hydroxy group together with water molecules connects the layers into a three-dimensional supramolecular network. From the solid-state structural standpoint, it can be concluded that the obtained ligands have robust electronic and geometric features, deviating slightly from the most symmetric ones due to intermolecular interactions or packing constraints. This is quite the opposite of the behavior in solution.

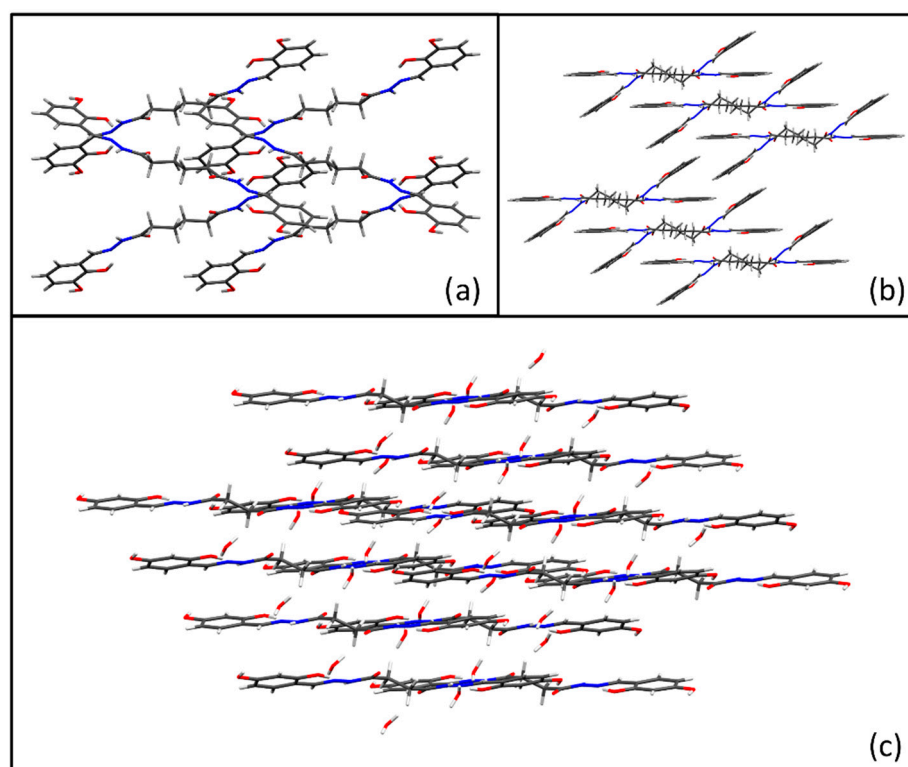


**Figure 3.** Crystal packing in: (a)  $\text{H}_4\text{L}^7$  viewed down the  $c$ -axis, (b)  $\text{H}_4\text{L}^6$  viewed down the  $b$ -axis, and (c)  $\text{H}_4\text{L}^4 \cdot 2\text{H}_2\text{O}$  viewed down the  $a$ -axis.

### 3.2. NMR Spectroscopy

Tautomeric equilibria and conformational space for compounds  $\text{H}_4\text{L}^1$ – $\text{H}_4\text{L}^8$  in  $\text{DMSO-}d_6$  solution were explored via NMR spectroscopy (Supplementary Material, Figures S37–S42). When carefully examining molecular structures of  $\text{H}_4\text{L}^1$ – $\text{H}_4\text{L}^8$ , it is clear that they can afford several tautomeric forms (Supplementary Material, Schemes S2 and S3). Due to intramolecular  $\text{O-H}\cdots\text{N}$  proton transfer, typical for *ortho*-hydroxy Schiff bases and aroylhydrazones, aldehyde residues of each subunit of  $\text{H}_4\text{L}^1$ – $\text{H}_4\text{L}^8$  can exist in the enol-imino or keto-amino tautomeric form (Supplementary Material, Schemes S2 and S3). Additionally, hydrazone functionality can undergo tautomeric equilibrium to yield the  $\text{N-NH-C=O}$  or  $\text{N-N=C-OH}$  form (Supplementary Material, Schemes S2 and S3). For the evaluation of such complex systems in solution, techniques of multinuclear ( $^1\text{H}$ ,  $^{13}\text{C}$ ,  $^{15}\text{N}$ ) NMR spectroscopy are irreplaceable and regularly employed [36,38,41–46]. Namely, nitrogen chemical shifts,  $\delta_{\text{N}}$ , as well as carbon signals,  $\delta_{\text{C}}$ , of the functionalities involved in the tautomerization will greatly differ. For example, the pure enol-imino form (considering aldehyde residues), where no intramolecular  $\text{O-H}\cdots\text{N}$  hydrogen bonding occurs, will expectedly give  $\delta_{\text{N}}$  signals around 330 ppm (referenced to the  $\text{NH}_3(\text{l})$ ). In the case of intramolecular  $\text{O-H}\cdots\text{N}$  hydrogen bond formation, the imine nitrogen  $\delta_{\text{N}}$  signal will be shifted upfield, to ca. 280 ppm. However, the change in the tautomeric form will cause a dramatic  $\delta_{\text{N}}$  upfield shift to values ranging from 140 ppm to 180 ppm. A comparable situation is observed for the carbon signals,  $\delta_{\text{C}}$ , where typical values for the pure enol-imino form are  $\approx 150$  ppm, whereas those for the pure keto-amino form are expected to appear at about 180 ppm. However, one must keep in mind that, in the case of fast conversion of tautomers, only one set of signals,  $\delta_{\text{N}}$  and  $\delta_{\text{C}}$ , will appear, reflecting the time- and space-averaged contribution of each tautomer in the mixture. Similarly, shifts of  $\delta_{\text{N}}$  and  $\delta_{\text{C}}$  are expected to follow the change in the tautomeric form, i.e.,  $\text{N-NH-C=O}/\text{N-N=C-OH}$ , of the hydrazone functionality. For the investigated compounds,  $\delta_{\text{N}}$  values appear at  $\approx 300$  ppm and at  $\approx 170$  ppm for N1 and N2 atoms, respectively (Supplementary Material, Table S5 and S6). On the other hand, values of  $\delta_{\text{C}}$  for the C2 and C8 atoms are found at  $\approx 140$  ppm and at  $\approx 170$  ppm, respectively (Sup-

plementary Material, Table S5 and S6). This reveals that, in DMSO- $d_6$  solution,  $H_4L^1$ – $H_4L^8$  predominantly occur as enol-imino tautomers, when considering both of their aldehyde subunits, while the related hydrazone parts assume the N–NH–C=O form.

Besides the potential to yield several tautomeric forms,  $H_4L^1$ – $H_4L^8$  can also afford an impressive collection of isomers in solution (Supplementary Material, Schemes S2 and S3). The total number of isomers existing in the solution at a given temperature will depend on the energy barrier of the rotation around particular bonds, which again will be reflected in the rate of conversion between isomers. While the rotation around the carbon–nitrogen bond of the  $-(C=O)-NH-$  linkage will give rise to *cis* and *trans* isomers, the rotations about N–N and  $C_{ar}-CH$  are associated with the presence of *syn*, *anti*, *syn'*, and *anti'* conformers (Supplementary Material, Schemes S2 and S3) [23,47–51]. As expected by the presence of two subunits which can assume the same or different conformations, the NMR spectra of all compounds investigated here are extremely complex, showing that in each case there are several isomers/conformers present in the solution at 25 °C (Supplementary Material, Figures S37–S42). Namely, for compounds  $H_4L^1$ – $H_4L^3$  and  $H_4L^5$ – $H_4L^7$ , for some atoms, up to four sets of signals were observed, while for  $H_4L^4$  and  $H_4L^8$ , even six sets of signals could be distinguished (Supplementary Material, Tables S5 and S6). However, due to severe overlap of the corresponding signals, unambiguous assignment of the conformer types, without the aid of quantum chemical calculations, was not possible. Based on the comparison with the relevant literature data and considering significant spectral features, it seems reasonable to conclude that the detected isomers constitute two large groups, one of the *cis* and the other of the *trans* type, the *trans* one being more populated [47–50]. Within each group, we anticipate, there exist different isomers/conformers, *syn*, *anti*, and *syn'* (considering only one subunit), due to rotations around other available bonds (Supplementary Material, Schemes S2 and S3). Such a scenario is supported by the temperature-dependent NMR measurements, which reveal that heating of the DMSO solutions for  $H_4L^1$ – $H_4L^8$  from 25 °C to 75 °C results in convergence (coalescence) of signals, leaving in all cases only two sets of signals, one related to the group of *trans* isomer(s) and the other to the group of *cis* isomer(s) (Figure 4, Supplementary Material, Figures S43 and S44).

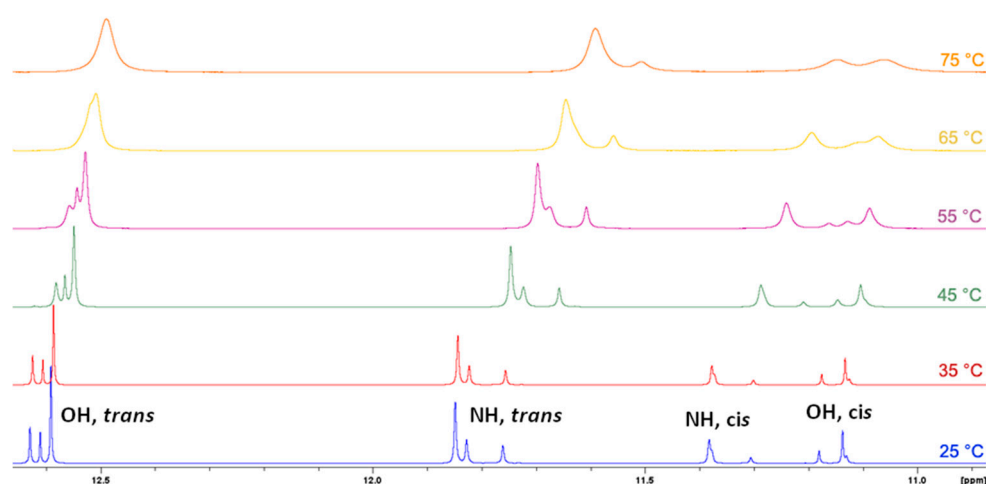


**Figure 4.** A portion of  $^1H$  NMR spectra of  $H_4L^2$  in DMSO- $d_6$  solution at different temperatures.

### 3.3. In Vitro Cytotoxic and Antibacterial Activity

The dihydrazones reported here were tested for their cytotoxic activity against THP-1 and HepG2 cells, and their antibacterial activity was assessed on *S. aureus*, *E. faecalis*, *E. coli*, and *M. catarrhalis* bacterial strains. The bioassay results are summarized in Table 1.

**Table 1.** The IC<sub>50</sub> values and minimum inhibitory concentrations (MIC) of the dihydrazones.

Compound	IC <sub>50</sub> /μmol L <sup>-1</sup>		MIC (μg mL <sup>-1</sup> )			
	THP-1	HepG2	<i>S. aureus</i>	<i>E. faecalis</i>	<i>E. coli</i>	<i>M. catarrhalis</i>
H <sub>4</sub> L <sup>1</sup>	>100	>100	>256	64	>256	16
H <sub>4</sub> L <sup>2</sup>	>100	>100	>256	16	128	8
H <sub>4</sub> L <sup>3</sup>	>100	>100	>256	>256	>256	128
H <sub>4</sub> L <sup>4</sup>	>100	>100	>256	>256	>256	>256
H <sub>4</sub> L <sup>5</sup>	>100	>100	>256	16	>256	256
H <sub>4</sub> L <sup>6</sup>	>100	>100	>256	16	16	16
H <sub>4</sub> L <sup>7</sup>	>100	>100	>256	>256	>256	>256
H <sub>4</sub> L <sup>8</sup>	>100	>100	>256	>256	>256	128
staurosporine	0.32	30.75	-	-	-	-
azithromycin	-	-	2	8	0.25	0.25

The determined IC<sub>50</sub> values (the concentration of the compound required to decrease cell viability by 50%) higher than 100 μmol L<sup>-1</sup> show that all of the examined dihydrazones can be considered non-cytotoxic against the THP-1 and HepG2 cell lines. This result encouraged us to investigate the antibacterial activity of these compounds. In general, MIC values (the lowest concentration at which no growth of bacteria is observed) equal to 64 mg mL<sup>-1</sup> or higher indicate that the examined dihydrazones show negligible or no antibacterial activity towards the tested bacterial isolates. Furthermore, some of the tested dihydrazones with MICs in the range 8–16 mg mL<sup>-1</sup> demonstrate selective activity against *M. catarrhalis* and *E. faecalis* which can be characterized as substantial to intermediate. However, the anti-*M. catarrhalis* activity of these compounds is notably lower when compared to the relevant antibiotic azithromycin. When the effect of the aldehyde moiety on the activity is compared, the highest activity is exhibited by the dihydrazones derived from 1-hydroxy-2-naphthaldehyde and salicylaldehyde, while those originating from 3-hydroxy- and 4-hydroxysalicylaldehyde show the lowest activity. The enhanced antibacterial activity of H<sub>4</sub>L<sup>1</sup>, H<sub>4</sub>L<sup>2</sup>, H<sub>4</sub>L<sup>5</sup>, and H<sub>4</sub>L<sup>6</sup> could be explained by the increased lipophilicity of these compounds and their easier passage through the cell membrane.

#### 4. Conclusions

Alkyl dihydrazones were straightforwardly prepared by condensation of succinyl or adipoyl dihydrazide with selected *ortho*-hydroxybenzaldehydes utilizing conventional solution synthesis. FTIR and structural studies in the solid state revealed the enol-imino tautomeric form of the aldehyde residues and a N–NH–C=O tautomeric form of the hydrazone functionalities. For the structurally characterized compounds, *trans-syn* conformation was established, with slight differences in molecular geometry. Unlike in the solid state, in DMSO-*d*<sub>6</sub> solution, molecules adopted several conformations while retaining the same tautomeric form, arising from rotations around C–N, N–N, and C<sub>ar</sub>–C bonds. This study clearly demonstrates the conformational richness for this class of compounds, which certainly deserves further research, including a wider set of compounds and support by quantum chemical calculations.

None of the dihydrazones caused cytotoxic effects on THP-1 and HepG2 cells under the tested conditions. Some of the dihydrazones reported herein showed moderate anti-*M. catarrhalis* and anti-*E. faecalis* activity. These results suggest that the further modification of this type of compound could lead to new agents with enhanced antibacterial ability.

**Supplementary Materials:** The following supporting information can be downloaded at: <https://www.mdpi.com/article/10.3390/cryst12081175/s1>, Table S1: General and crystallographic data; Tables S2 and S3: Selected bond lengths and angles; Table S4: Geometry of hydrogen bonds and π···π interactions; Figures S1–S9: TGA and DSC thermograms; Figures S10–S17: IR-ATR spectra; Figures S18–S21: Comparison of PXRD patterns; Figures S22–S24: Molecular structures; Figures S25–S36:

Crystal packings; Schemes S1 and S2: Structures and the NMR numbering schemes; Tables S5 and S6:  $^1\text{H}$  and  $^{13}\text{C}$  and  $^{15}\text{N}$  assignments; Figures S37–S44: NMR spectra.

**Author Contributions:** Investigation, formal analysis, writing—original draft preparation, E.T., V.D., K.P. and M.R.; visualization, E.T. and M.R., writing—review and editing, E.T., V.D., K.P., M.R. and V.V.; funding acquisition, project administration, supervision, V.V. All authors have read and agreed to the published version of the manuscript.

**Funding:** This work has been fully supported by the Croatian Science Foundation under the project (IP-2016-06-4221).

**Institutional Review Board Statement:** Not applicable.

**Informed Consent Statement:** Not applicable.

**Data Availability Statement:** Crystallographic datasets for the structures  $\text{H}_4\text{L}^4 \cdot 2\text{H}_2\text{O}$ ,  $\text{H}_4\text{L}^6$ , and  $\text{H}_4\text{L}^7$  are available through the Cambridge Structural Database with deposition numbers CCDC 2093077–2093079. These data can be obtained free of charge via <https://www.ccdc.cam.ac.uk/structures/>, accessed on 30 July 2022.

**Acknowledgments:** We are grateful to Ljubica Ljubić, Kristina Prezelj, mag. chem., for assistance in the synthetic procedures and Nikola Cindro for help with the NMR measurements. We acknowledge the support of project CluK co-financed by the Croatian Government and the European Union through the European Regional Development Fund—Competitiveness and Cohesion Operational Program (Grant KK.01.1.1.02.0016).

**Conflicts of Interest:** The authors declare no conflict of interest.

## References

1. Tatum, L.A.; Su, X.; Aprahamian, I. Simple Hydrazone Building Blocks for Complicated Functional Materials. *Acc. Chem. Res.* **2014**, *47*, 2141–2149. [[CrossRef](#)] [[PubMed](#)]
2. Hussain, I.; Ali, A. Exploring the Pharmacological Activities of Hydrazone Derivatives: A Review. *J. Phytochem. Biochem.* **2017**, *1*, 1–11.
3. Sonawane, S.J.; Kalhapure, R.S.; Govender, T. Hydrazone Linkages in pH Responsive Drug Delivery Systems. *Eur. J. Pharm. Sci.* **2017**, *99*, 45–65. [[CrossRef](#)] [[PubMed](#)]
4. Busschaert, N.; Caltagirone, C.; Van Rossom, W.; Gale, P.A. Applications of Supramolecular Anion Recognition. *Chem. Rev.* **2015**, *115*, 8038–8155. [[CrossRef](#)]
5. Su, X.; Aprahamian, I. Hydrazone-based switches, metallo-assemblies and sensors. *Chem. Soc. Rev.* **2014**, *43*, 1963–1981. [[CrossRef](#)]
6. Van Dijken, D.J.; Kovariček, P.; Ihrig, S.P.; Hecht, S. Acylhydrazones as Widely Tunable Photoswitches. *J. Am. Chem. Soc.* **2015**, *137*, 14982–14991. [[CrossRef](#)]
7. Li, L.-Y.; Peng, J.-D.; Zhou, W.; Qiao, H.; Deng, X.; Li, Z.-H.; Li, J.-D.; Fu, Y.-D.; Li, S.; Sun, K.; et al. Potent Hydrazone Derivatives Targeting Esophageal Cancer Cells. *Eur. J. Med. Chem.* **2018**, *148*, 359–371. [[CrossRef](#)]
8. Verma, G.; Marella, A.; Shaquiquzzaman, M.; Akhtar, M.; Rahmat Ali, M.; Mumtaz Alam, M. A review exploring biological activities of hydrazones. *J. Pharm. Bioallied Sci.* **2014**, *6*, 69–80.
9. Rollas, S.; Küçükgül, S.G. Biological activities of hydrazone derivatives. *Molecules* **2007**, *12*, 1910–1939. [[CrossRef](#)]
10. De Oliveira Carneiro Brum, J.; Costa França, T.C.; LaPlante, S.R.; Figueroa Villar, J.D. Synthesis and Biological Activity of Hydrazones and Derivatives: A Review. *Mini-Rev. Med. Chem.* **2020**, *20*, 342–368. [[CrossRef](#)]
11. Ullah, H.; Previtali, V.; Mihigo, H.B.; Twamley, B.; Rauf, M.K.; Javed, F.; Waseem, A.; Baker, R.J.; Rozas, I. Structure-activity relationships of new Organotin(IV) anticancer agents and their cytotoxicity profile on HL-60, MCF-7 and HeLa human cancer cell lines. *Eur. J. Med. Chem.* **2019**, *181*, 111544. [[CrossRef](#)] [[PubMed](#)]
12. Omid, S.; Kakanejadifard, A. A review on biological activities of Schiff base, hydrazone, and oxime derivatives of curcumin. *RSC Adv.* **2020**, *10*, 30186–30202. [[CrossRef](#)] [[PubMed](#)]
13. Wahbeh, J.; Milkowski, S. The Use of Hydrazones for Biomedical Applications. *SLAS Technol.* **2019**, *24*, 161–168. [[CrossRef](#)]
14. Ray, D.; Foy, J.T.; Hughes, R.P.; Aprahamian, I. A switching cascade of hydrazone-based rotary switches through coordination-coupled proton relays. *Nat. Chem.* **2012**, *4*, 757–762. [[CrossRef](#)] [[PubMed](#)]
15. Ruben, M.; Lehn, J.-M.; Müller, P. Addressing metal centres in supramolecular assemblies. *Chem. Soc. Rev.* **2006**, *35*, 1056–1067. [[CrossRef](#)]
16. Hardy, J.G. Metallo-supramolecular grid complexes: Towards nanostructured materials with high-tech applications. *Chem. Soc. Rev.* **2013**, *42*, 7881–7899. [[CrossRef](#)]
17. Zhao, L.; Niel, V.; Thompson, L.K.; Xu, Z.; Milway, V.A.; Harvey, R.G.; Miller, D.O.; Wilson, C.; Leech, M.; Howard, J.A.K.; et al. Self-assembled polynuclear clusters derived from some flexible polydentate dihydrazide ligands. *Dalton Trans.* **2004**, *9*, 1446–1455. [[CrossRef](#)]

18. Stadler, A.-M.; Harrowfield, J. Bis-acyl-/aroyl-hydrazones as multidentate ligands. *Inorg. Chim. Acta* **2009**, *362*, 4298–4314. [[CrossRef](#)]
19. Lu, C.; Htan, B.; Ma, C.; Liao, R.-Z.; Gan, Q. Acylhydrazone Switches: *E/Z* Stability Reversed by Introduction of Hydrogen Bonds. *Eur. J. Org. Chem.* **2018**, *48*, 7046–7050. [[CrossRef](#)]
20. Landge, S.M.; Tkatchouk, E.; Benítez, D.; Lanfranchi, D.A.; Elhabiri, M.; Goddard, W.A.; Aprahamian, I. Isomerization Mechanism in Hydrazone-Based Rotary Switches: Lateral Shift, Rotation, or Tautomerization? *J. Am. Chem. Soc.* **2011**, *133*, 9812–9823. [[CrossRef](#)]
21. Cvrtila, I.; Fanlo-Virgós, H.; Schaeffer, G.; Monreal Santiago, G.; Otto, S. Redox Control over Acyl Hydrazone Photoswitches. *J. Am. Chem. Soc.* **2017**, *139*, 12459–12465. [[CrossRef](#)] [[PubMed](#)]
22. Borthakur, R.; Kumar, A.; Lemtur, A.; Lal, R.A. Synthesis, characterization and electrochemical properties of bis( $\mu^2$ -perchlorato)tricopper(II) complexes derived from succinoyldihydrazones. *RSC Adv.* **2013**, *3*, 15139–15147. [[CrossRef](#)]
23. Ranford, J.D.; Vittal, J.J.; Wang, Y.M. Dicopper(II) Complexes of the Antitumor Analogues Acylbis(salicylaldehyde hydrazones) and Crystal Structures of Monomeric  $[\text{Cu}_2(1,3\text{-propanedioyl bis(salicylaldehydehydrazone))(\text{H}_2\text{O})_2] \cdot (\text{ClO}_4)_2 \cdot 3\text{H}_2\text{O}$  and Polymeric  $[\{\text{Cu}_2(1,6\text{-hexanedioyl bis(salicylaldehydehydrazone))(\text{C}_2\text{H}_5\text{OH})_2\}_m] \cdot (\text{ClO}_4)_{2m} \cdot m(\text{C}_2\text{H}_5\text{OH})$ . *Inorg. Chem.* **1998**, *37*, 1226–1231. [[PubMed](#)]
24. Popiołek, Ł. Hydrazone–hydrazones as potential antimicrobial agents: Overview of the literature since 2010. *Med. Chem. Res.* **2017**, *26*, 287–301. [[CrossRef](#)]
25. Kumar, P.; Narasimhan, B. Hydrazides/hydrazones as antimicrobial and anticancer agents in the new millennium. *Mini Rev. Med. Chem.* **2013**, *13*, 971–987. [[CrossRef](#)] [[PubMed](#)]
26. Shujah, S.; Khalid, N.; Ali, S. Homobimetallic Organotin(IV) Complexes with Succinohydrazone Schiff Base: Synthesis, Spectroscopic Characterization, and Biological Screening. *Russ. J. Gen. Chem.* **2017**, *87*, 515–522. [[CrossRef](#)]
27. Sedaghat, T.; Aminian, M.; Bruno, G.; Amiri Rudbari, H. Binuclear organotin(IV) complexes with adipic dihydrazones: Synthesis, spectral characterization, crystal structures and antibacterial activity. *J. Organomet. Chem.* **2013**, *737*, 26–31. [[CrossRef](#)]
28. Sharma, M.P.; Varshney, V.K.; Sharma, R.C. Synthesis and antimicrobial study of some hydrazone metal complexes. *Proc. Natl. Acad. Sci. USA* **1991**, *61*, 447–452.
29. González-García, C.; Mata, A.; Zani, F.; Antonia Mendiola, M.; López-Torres, E. Synthesis and antimicrobial activity of tetradentate ligands bearing hydrazone and/or thiosemicarbazone motifs and their diorganotin(IV) complexes. *J. Inorg. Biochem.* **2016**, *163*, 118–130. [[CrossRef](#)]
30. *CrysAlisPro Software System*, version 1.171.41.92a; Rigaku Oxford Diffraction: Oxford, UK, 2020.
31. Sheldrick, G.M. SHELXT-Integrated space-group and crystal-structure determination. *Acta Cryst. A* **2015**, *71*, 3–8. [[CrossRef](#)]
32. Sheldrick, G.M. Crystal structure refinement with SHELXL. *Acta Cryst. C* **2015**, *71*, 3–8. [[CrossRef](#)] [[PubMed](#)]
33. Dolomanov, O.V.; Bourhis, L.J.; Gildea, R.J.; Howard, J.A.K.; Puschmann, H. OLEX2: A complete structure solution, refinement and analysis program. *J. Appl. Cryst.* **2009**, *42*, 339–341. [[CrossRef](#)]
34. Macrae, C.F.; Sovago, I.; Cottrell, S.J.; Galek, P.T.A.; McCabe, P.; Pidcock, E.; Platings, M.; Shields, G.P.; Stevens, J.S.; Towler, M.; et al. Mercury 4.0: From visualization to analysis, design and prediction. *J. Appl. Cryst.* **2020**, *53*, 226–235. [[CrossRef](#)] [[PubMed](#)]
35. Mosmann, T. Rapid colorimetric assay for cellular growth and survival: Application to proliferation and cytotoxicity assays. *J. Immunol. Methods* **1983**, *65*, 55–63. [[CrossRef](#)]
36. Rubčić, M.; Pisk, J.; Pičuljan, K.; Damjanović, V.; Lovrić, J.; Vrdoljak, V. Symmetrical disubstituted carbohydrazides: From solid-state structures to cytotoxic and antibacterial activity. *J. Mol. Struct.* **2019**, *1178*, 222–228. [[CrossRef](#)]
37. *CLSI Document M07-A8, Methods for Dilution Antimicrobial Susceptibility Tests for Bacteria that Grow Aerobically*; Clinical and Laboratory Standards Institute: Wayne, PA, USA, 2009.
38. Rubčić, M.; Galić, N.; Halasz, I.; Jednačak, T.; Judaš, N.; Plavec, J.; Šket, P.; Novak, P. Multiple solid forms of 1,5-bis(salicylidene)carbohydrazide: Polymorph-modulated thermal reactivity. *Cryst. Growth Des.* **2014**, *14*, 2900–2912. [[CrossRef](#)]
39. Borthakur, R.; Kumar, A.; Lal, R.A. Synthesis and characterization of heterotrinary bis( $\mu^2$ -chlorido)dicopper (II) mono zinc(II) complexes derived from succinoyldihydrazones. *Spectrochim. Acta A Mol. Biomol. Spectrosc.* **2014**, *118*, 94–101. [[CrossRef](#)]
40. Etter, M.C.; MacDonald, J.C.; Bernstein, J. Graph-set analysis of hydrogen-bond patterns in organic crystals. *Acta Cryst. B* **1990**, *46*, 256–262. [[CrossRef](#)]
41. Hansen, P.E.; Rozwadowski, Z.; Dziembowska, T. NMR Studies of Hydroxy Schiff Bases. *Curr. Org. Chem.* **2009**, *13*, 194–215. [[CrossRef](#)]
42. Claramunt, R.M.; López, C.; Santa María, M.D.; Sanz, D.; Elguero, J. The use of NMR spectroscopy to study tautomerism. *Prog. Nucl. Magn. Reson. Spectrosc.* **2006**, *49*, 169–206. [[CrossRef](#)]
43. Novak, P.; Jednačak, T.; Parlov Vuković, J.; Zangger, K.; Rubčić, M.; Galić, N.; Hrenar, T. Synthesis, Structural Characterization and Hydrogen Bonding of Mono(salicylidene)carbohydrazide. *Croat. Chem. Acta* **2012**, *85*, 451–456. [[CrossRef](#)]
44. Schilf, W.; Kamieński, B.; Užarević, K. Nitrogen and carbon CP/MAS NMR investigations of keto–enol tautomerism in asymmetric o-hydroxy Schiff bases. *J. Mol. Struct.* **2013**, *1031*, 211–215. [[CrossRef](#)]
45. Užarević, K.; Rubčić, M.; Stilinović, V.; Kaitner, B.; Cindrić, M. Keto–enol tautomerism in asymmetric Schiff bases derived from p-phenylenediamine. *J. Mol. Struct.* **2010**, *984*, 232–239. [[CrossRef](#)]
46. Božić, A.R.; Filipović, N.R.; Verbić, T.Ž.; Milčić, M.K.; Todorović, T.R.; Cvijetić, I.N.; Klisurić, O.R.; Radišić, M.M.; Marinković, A.D. A detailed experimental and computational study of monocarbohydrazones. *Arab. J. Chem.* **2020**, *13*, 932–953. [[CrossRef](#)]

47. Caprice, K.; Aster, A.; Coughon, F.B.L.; Kumpulainen, T. Untying the Photophysics of Quinolinium-Based Molecular Knots and Links. *Chem. Eur. J.* **2020**, *26*, 1576–1587. [[CrossRef](#)] [[PubMed](#)]
48. Fischer, G. Chemical aspects of peptide bond isomerisation. *Chem. Soc. Rev.* **2000**, *29*, 119–127. [[CrossRef](#)]
49. Hamzi, I.; Barhoumi-Slimi, T.M.; Abidi, R. Synthesis, Characterization, and Conformational Study of Acylhydrazones of  $\alpha,\beta$ -Unsaturated Aldehydes. *Heteroat. Chem.* **2016**, *27*, 139–148. [[CrossRef](#)]
50. Kumar, P.; Kadyan, K.; Duhan, M.; Sindhu, J.; Singh, V.; Singh Saharan, B. Design, synthesis, conformational and molecular docking study of some novel acyl hydrazone based molecular hybrids as antimalarial and antimicrobial agents. *Chem. Cent. J.* **2017**, *11*, 115. [[CrossRef](#)]
51. In principle, *E/Z* isomerisation can also occur in hydrazones. However, this process usually proceeds under the influence of external stimuli, e.g., UV irradiation, and it is crucial that structure contains functionality that can stabilize generally less stable *Z* isomer through e.g., intramolecular hydrogen bond. For example see references 1, 5, 14 and 20. For the structures investigated here, the observed chemical shifts do not suggest the occurrence of *Z* isomer in solution. Also considering the structure of molecules, occurrence of *Z* isomer here should be disfavored due to the sterical hindrance it should sustain.